Quadrupole Interaction in Metals: Nuclear Methods*

H. Haas

Hahn-Meitner-Institut Berlin and Freie Universität Berlin, Germany

Z. Naturforsch. **41 a**, 78–90 (1986); received October 3, 1985

Nuclear techniques offer the unique possibility to investigate the hyperfine interaction at isolated impurities in matter. Electric field gradients at impurities in metals have now been determined in numerous systems. An overview of the various techniques – perturbed angular correlation/distribution, Mössbauer spectroscopy, nuclear orientation – is presented. For sp-impurities in simple metals the results show a very clear pattern that can be understood in terms of the local density of states. Several recent applications of nuclear methods to more complicated systems like alloys, point defects, diffusion, and surfaces are discussed.

A) Methods

1. Historical Introduction

One of the most important discoveries of atomic physics was the observation of the splitting of optical lines by the interaction of the electrons with the nuclear moments. For many years the measurement of this hyperfine interaction was only possible in free atoms. The determination of nuclear spins, magnetic moments, and later quadrupole moments of stable ground states has been very important in the process of achieving an understanding of the structure of nuclei.

The detection of NMR in condensed matter [1] opened up a completely new field, the use of nuclear moments in the investigation of liquids and solids. Four years later followed the first determinations of quadrupole coupling constants [2]. The electric field gradient, EFG, is actually one of the most informative aspects of hyperfine interactions in solids we know today.

Not very long after the discovery of NMR/NQR several new methods (perturbed angular correlation PAC [3], nuclear orientation NO [4], perturbed angular distribution PAD [5], β-NMR [6], etc.) were invented to extend the nuclear moment measurements to radioactive nuclei and shortlived excited states, generally in condensed matter. Since for these techniques, however, the handling of radioactivity or the use of particle accelerators was necessary, only few laboratories could perform such experiments. When the Mößbauer effect was discovered [7], if found almost immediate widespread application, largely due to the fact that the solid samples studied did not have to contain radioactivity.

The steady improvement in experimental equipment and facilities has now led to the situation that all the nuclear techniques, historically more directed toward nuclear moment measurements, can be routinely applied for solid state studies. Since generally only a small number of probe atoms (10^8–10^{14}) are needed and high energy radiation is detected, these methods are especially suited for the investigation of impurities, primarily in metals. The internal magnetic field at impurities are of great value in all studies of magnetism, a very active area of solid state physics at present. This review is concerned with the quadrupole interaction at impurities in metals, perhaps the most important contribution of the nuclear methods, particularly when the many applications are considered.

2. Overview of Methods

In all studies of hyperfine interactions in solids one measures the splitting of the nuclear sublevels in the field acting on the nucleus. The techniques may be classified according to the way in which these energy separations, typically of order 100 MHz, are determined:

a) Direct spectroscopy (NMR/NQR): Quanta corresponding to the transition energy are absorbed, emitted or scattered by the system. For RF spectroscopy the sensitivity is very low, making a large

---

* Presented at the VIIIth International Symposium on Nuclear Quadrupole Resonance Spectroscopy, Darmstadt, July 22–26, 1985.

Reprint requests to Herrn Dr. H. Haas, Hahn-Meitner-Institut Berlin, Glienicker-Str. 100, 1000 Berlin 39.

0340-4811 / 86 / 0100-0078 $ 01.30/0. – Please order a reprint rather than making your own copy.

sample necessary. The accuracy and resolution of these techniques is generally ideal, limited only by the properties of the solid investigated.

b) Indirect spectroscopy (MS, OS, ESR): Quanta of higher energy (γ-ray, optical, microwave) are used to detect the splitting via high resolution spectroscopy, thus increasing the sensitivity considerably. In Mössbauer spectroscopy (MS) quanta of typically 40 keV are detected, with a splitting of 100 MHz equivalent to $\sim 0.4\,\mu$eV, thus requiring 10^{-11} resolution. This is obtainable by Doppler tuning of source and absorber with a velocity drive. The ultimate limit to accuracy and resolution due to the nuclear state lifetime ($\sim 1\,\mu$s) is typically 1 MHz.

c) Thermal population (NO): At low enough temperatures (100 MHz corresponds to ~ 5 mK) the thermal population of the sublevels differs considerably. This leads to anisotropic emission of the high energy nuclear decay radiation (α, β, γ, e^-). Analysis of this effect can give the splittings with a typical accuracy of 10%. Similarly for stable nuclei in bulk samples the effect of the splitting on the specific heat may be observed.

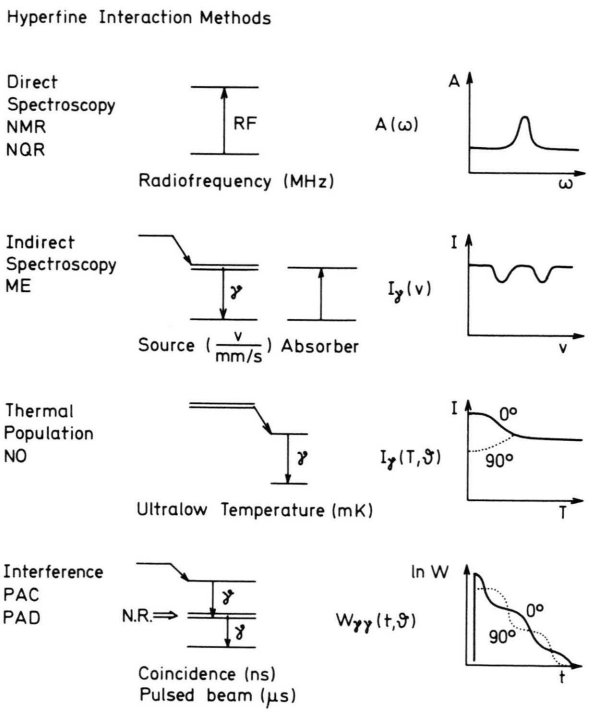

Fig. 1. Schematic summary of hyperfine interaction methods.

d) Interference (PAC/PAD): Coherent production of the nuclear sublevels in nuclear reactions or decay leads to a time-dependent interference pattern in the subseuent decay, the beat period for a 100 MHz splitting being 10 ns. The nuclear lifetimes (1 ns to 10 ms) generally limit accuracy and resolution. A related technique, where not nuclear but optical transitions are observed, is known under the name of quantum beat spectroscopy.

Of course, these basic techniques can the be combined in various ways to enhance sensitivity or resolution. The well known ENDOR spectroscopy provides the classical example as a combination of ESR and NMR. The most important nuclear combined technique is probably β-NMR, where long-lived β-active nuclei are produced in a polarized state and the NMR destruction of this polarization is monitored via the β-anisotropy, combining nuclear sensitivity with NMR precision. Naturally all the methods mentioned here are described in detail with many technical variants in the literature [8, 9]. In Fig. 1 the basic techniques are sketched graphically in a uniform way to facilitate comparison

3. PAC/PAD Basics

While the basic principles of NMR/NQR and MS are well known by now and those of NO are quite straightforward, the PAC/PAD method has not yet reached the textbook level and needs some introductory explanation. It shall be described here in simple physical terms. Elegant spherical tensor density matrix descriptions of the full theory are available in review articles [10].

The concept of angular correlation in a γ-γ-cascade can easily be explained for the simplest example, a spin sequence of 0-1-0. The first γ-transition produces the intermediate state only in the $m = \pm 1$ substates in the coordinate system along the emission direction z, since the photon has to carry one unit of angular momentum. For the same reason the second decay γ is then emitted preferentially parallel or antiparallel to z. An angular correlation of the form $W(\theta_{12}) = 1 + A_{22} P_2(\cos\theta_{12})$ describes this behaviour. The correct coefficient $A_{22} = 0.5$ is obtained if one realizes that the $m = 0$ intermediate state would not be able to emit into the z-direction at all, and equal population of $m = -1, 0, +1$ would give isotropy. For more com-

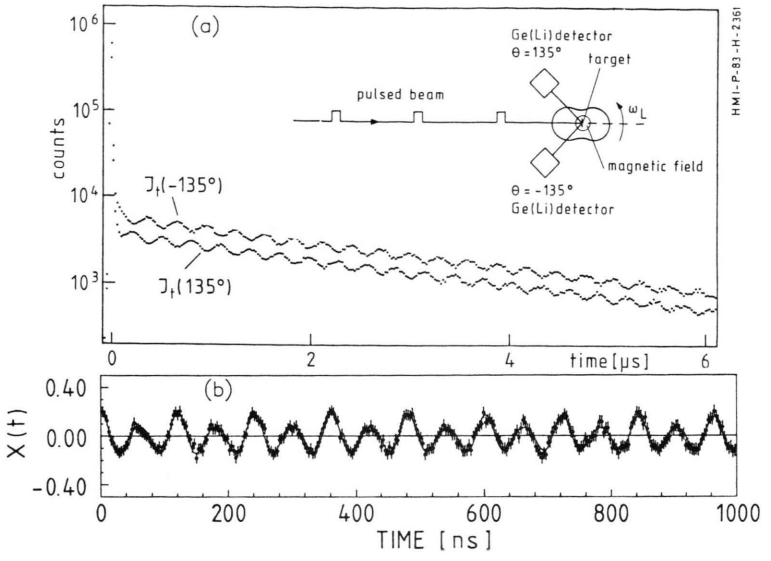

Fig. 2. a) Typical PAD experiments for magnetic interaction. b) Typical quadrupole modulation (autocorrelation function).

plicated spin sequences vector coupling theory results in a somewhat complex angular correlation, with the contributions of higher order Legendre polynomials P_4, P_6 generally being small, however.

For a lifetime τ of the intermediate state of the cascade the coincidence rate for two detectors at an angle θ will be of the form

$$W(\theta, t) = e^{-t/\tau}[1 + A_{22} P_2(\cos\theta)],$$

experimentally measurable for τ in the ns to μs range. If one then applies a magnetic field B perpendicular to the detector plane, the initial anisotropy distribution, coupled to the intermediate nuclear spin system, will rotate with the Larmor precession $\omega_L = \mu B/i\hbar$, giving

$$W(\theta, t) = e^{-t/\tau}[1 + A_{22} P_2(\cos(\theta + \omega_L t))] .$$

The perturbation thus yields a periodic modulation of the coincidence rate as function of time that is measured in such a "spin rotation" experiment. The modulation frequency is $2\omega_L$ to lowest order, corresponding to a $\Delta m = 2$ transition in NMR. In Fig. 2a the PAD variant of this technique is shown as example. Here the isomeric nuclear state is populated and aligned by a pulsed accelerator beam, thus eliminating the need for a coincidence and enabling measurements of very longlived (ms) states.

It is also possible to study nuclear quadrupole interactions by these methods. Since $\pm m$ are populated equally, however, not net precession results but only a "breathing" of the angular distribution at different frequencies due to the unequal sublevel splitting. A typical perturbation in a single crystal obtained after elimination of the trivial effects of the exponential decay is shown in Figure 2b. If randomly oriented EFG's are present, an even more complex pattern results containing $\Delta m = 2, 1, 0$ components. Some special variants of PAC/PAD also allow to determine the sign of the quadrupole coupling through the production of nuclear polarization via β-decay [11], Coulomb [12] or surface scattering [13].

4. Modern Facilities

A common requirement for all nuclear methods is the preparation of samples containing the radioactive probe atoms. It is in most cases very difficult and time consuming to use classical radiochemical techniques for this purpose. The implantation process has been widely used in recent years as the most universal way to produce samples, particularly for metals. There are basically three possibilities:

a) Activation where the sample is used as a target for a nuclear reaction like (n, γ), (p, n) and the products are stopped internally.

b) Mass separators, where the ionized radioactive atoms are accelerated (typically to 50 keV) and implanted to a depth of typically 100 Å. The most powerful of such facilities are on-line with an intense beam of primary particles, like 600 MeV

protons for ISOLDE at CERN [14]. This is particularly important when short source halflives (seconds to hours) are involved.

c) Heavy ion accelerators like VICKSI at HMI Berlin [15], e.g., where the products of nuclear reactions with thin targets are recoil implanted into a backing at typically 5 MeV. Heavy ion reactions like (^{16}O, 3n) have also been used in many cases to implant shortlived isomers for PAD experiments into a metallic matrix.

5. Probe Elements

The ~ 60 possible probe elements for conventional NMR/NQR are practically all well known. Only some variants using nuclear detection have not been fully explored. The same is true for the ~ 20 suitable isotopes for MS. Even if new cases would be found, they are likely not to be of practical importance. For PAC this is not at all the case yet. The availability of shortlived sources will probably expand the present spectrum considerably. The use of more sophisticated instruments like electron spectrometers or semiconductor detectors will be necessary for most cases, however. The same is true for PAD, particularly for the heavier elements. Virtually all elements with $Z > 18$ have candidate levels for this technique. The low temperature NO method is also applicable for almost all elements, especially when combined with on-line implantation. The completion of the systematic study of EFG's in non-cubic metals can benefit very much from such measurements. Due to the formidable technical and principal problems of this technique, however, it will most likely not be very useful in the study of the more complex materials of interest in the future. With some exceptions the same is true for PAD.

6. Nuclear Quadrupole Moments

One of the major problems in obtaining EFG's by nuclear methods is the determination of the nuclear quadrupole moments, as only the product $e^2 Qq$ is measured. Considerable progress has been made in this respect, however, during the last 20 years.

Stable groud state accuracies of 1% have been obtained in many cases, generally by muonic X-ray spectroscopy. Also the values derived from atomic spectroscopy are now reliable to within 5% in most cases. If then the stable and a radioactive nucleus have been studied in the same matrix, the frequency ratio fixes the quadrupole moment.

Unfortunately such experiments are not availbale for all cases. For many elements the chain of data still contains a "missing link". It is then necessary to make use of some other information:

a) Nuclear theory can be used to relate the quadrupole moment for favourable cases to other measured parameters like transition strengths, yielding values accurate to 5–10%.

b) Nuclear systematics may give Q-values to 10–20% when the equivalent nuclear state has been measured for e.g. a neighbouring isotope.

c) Nuclear models are still now in a state that their predictions for quadrupole moments may only rarely be trusted to better than 10–30%.

d) EFG calculations for most systems can not yet be performed in a satisfactory way. Without guidance from experiments the accuracy rarely exceeds 20%, for metals sometimes not 50%.

For most nuclei of importance as probe elements reliable values are now available. In some cases, however, the accepted values had to be changed in recent years by factors up to 2.

B) Typical Examples

*1. Field Gradients in sp-Metals: ^{111}Cd**Cd***

The nuclear state that has found the most applications in nuclear studies of the quadrupole interaction is the first excited $5/2^+$ isomer of halflife 84 ns in ^{111}Cd. It may be populated in several ways as sketched in the level scheme of Figure 3a. Field gradients in a large number of systems have been determined by exploiting the various possibilities. The simplest matrix, Cd metal, has naturally been paid special attention, particularly since no stable Cd isotope with $I > 1/2$ is available. A typical modulation pattern from an in-beam PAD experiment is shown in Figure 3b. The interaction frequency can clearly be extracted with considerable accuracy. A the same time one can seen that at lower temperature some damping of the modulation is observed, coming from the frequency spread that has to be attributed to defects created in the metal during the implantation process [16]. This damping is absent for chemically prepared samples studied by γ-γ-PAC.

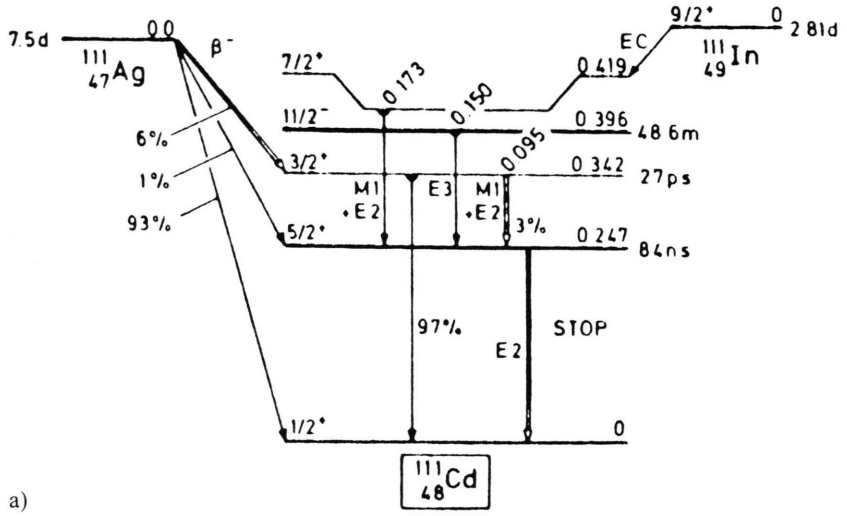

a)

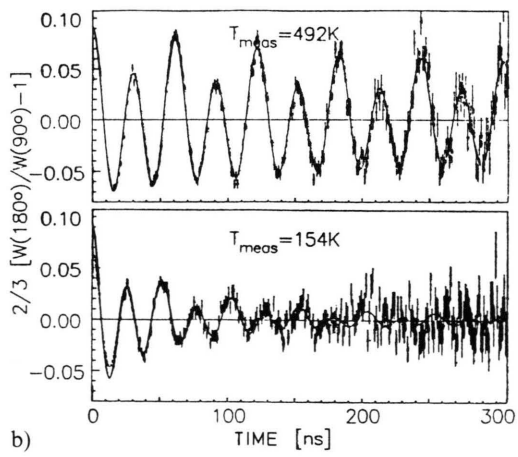

b)

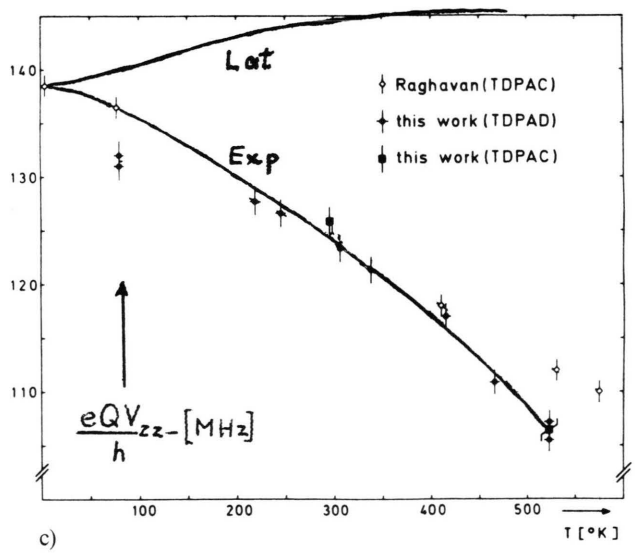

c)

Fig. 3. a) Level scheme of ^{111}Cd and ways of production. b) PAD modulation functions for ^{110}Cd(d, p)^{111}Cd**Cd**. c) Temperature dependence of coupling constant. Exp.: Intrinsic lattice value. Lat.: Result of point charge calculation.

Figure 3c shows an early example of a determination of the EFG temperature dependence by these methods. The deviations of the low temperature PAD data [17] from the intrinsic curve are connected with the defects mentioned above. At high temperatures the original PAC data [18] suffered from a trivial experimental problem. The temperature shift of the EFG in this and most other systems was observed to follow quite closely a $T^{1.5}$ dependence [19]. This effect is now believed to come from a somewhat fortituous interplay of the lattice expansion, a complex phonon spectrum and anharmonic thermal vibrations.

Since only high energy γ-quanta are observed, the PAC technique can also be applied to determine the effect of hydrostatic pressure and uniaxial stress [20] on the EFG. The results clearly show that the anisotropy of the nearest neighbour configuration in the crystal gives the dominating contribution.

For the $5/2^+$ isomer in ^{111}Cd the fortunate situation exists that three independent methods have been used to obtain the quadrupole moment:

a) Experimentally backed estimates of EFG's in selected ionic solids yield [21] $Q = 77$ fm^2;

b) PAD experiments on $11/2^-$ isomers in ^{107,109}Cd coupled with nuclear systematics give [22] $Q = 83$ fm^2;

c) low temperature NO for ^{111m}Cd**Zn** determines [23] $Q = +81$ fm^2.

The NO experiments and β-γ PAC data [11] clearly show a positive sign for $e^2 Qq/h$ and therefore a positive EFG $V_{zz} = +7.2 \cdot 10^{17}$ V/cm^2. This finding is in sharp contrast to the earlier used simple model of positive point charges at the atomic sites.

2. *Field Gradients in sp-Metals: Sn**Cd***

As already seen in the determination of the quadrupole moment of ^{111}Cd it is in many cases important to have several nuclear states of the same element available. A typical example for this are the Sn isotopes. With pulsed beam PAD measurements the coupling constants in Cd metal at ~ 550 K for isomeric states of ^{113,114,115,116,118}Sn were determined [24]. For the ^{118}Sn 10^+ isomer the quadrupole moment can be obtained reliably from the strength of the $10^+ - 8^+$ transition via nuclear theory. The temperature dependence, found to be similar to the Cd**Cd** case [25], thus allows to obtain the $T = 0$ value of the EFG by extrapolation as $V_{zz} = 9.8 \cdot 10^{17}$ V/cm^2. A positive sign of the EFG for Sn**Cd** and a negative one for Sn**Sb** results from analysis of the ^{119}Sn Mössbauer emission spectra of single crystals following ^{119}Cd implantation at ISOLDE [26] shown in Figure 4.

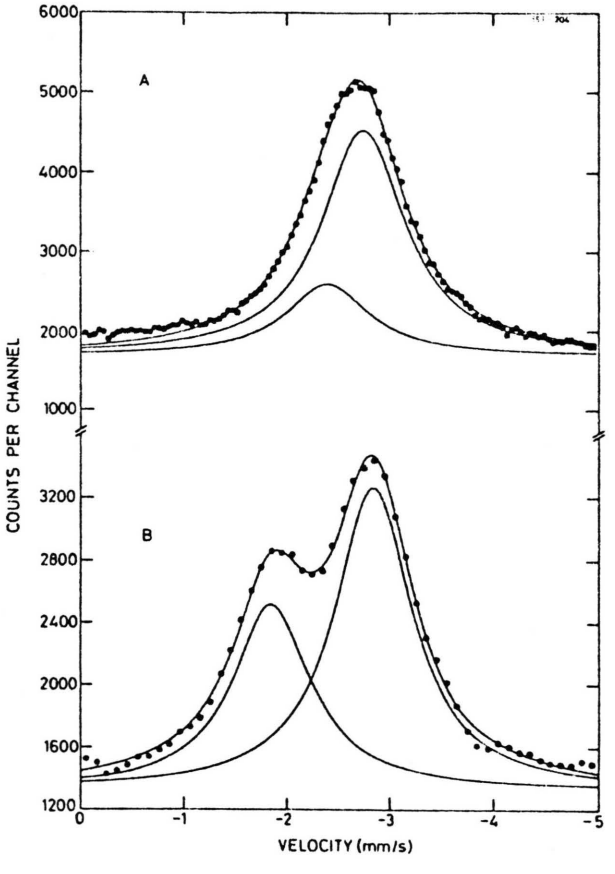

Fig. 4. Mössbauer emission spectra of ^{119}Cd → ^{119}In → ^{119}Sn. A: Sb ($\parallel$ c). B: Zn ($\perp$ c).

3. *Field Gradients in sp-Metals: ^{112}Sb**Cd***

The EFGs for Cd, In, Sn in Cd all have positive values of similar magnitude. Earlier data [27] gave some hint that something unusual happened for an Sb impurity atom. In Fig. 5 a PAD experiment performed at VICKSI is shown that clearly demonstrates this fact [28]. The 8^- isomer of ^{112}Sb was recoil implanted following ^{103}Rh(^{12}C, 3n) into a heated Cd single crystal. The very small modulation frequency gives $e^2 Qq/h = 5.9(2)$ MHz. If the c-axis of the crystal is turned into the beam direction the modulation disappears, thus proving that this is the EFG z-axis as required for a substitutional position. In this case the quadrupole moment involved could be fixed by a measurement of the ^{112}Sb isomer in Sb metal [29] and comparison with NQR data. The resulting EFG is more than an order of magnitude smaller than for the other 5 sp impurities in Cd, in complete disagreement with all expectations from previous systematics.

4. *Temperature Dependence of EFG: ^{79}Kr**Zn***

Since the EFG temperature dependence is thought to be dominated by lattice vibrations, a particularly strong effect could be expected for an impurity like a noble gas with very weak binding to the lattice and thus low frequency local vibrations. Up to 400 K a PAC experiment at ISOLDE on the $5/2^+$ state of ^{79}Kr gave the first evidence for the expected effect [30]. At higher temperatures, however, this measurement was not possible any more, apparently due to diffusion of the implanted ^{79}Rb activity. On the other hand, clean PAD spectra of the same isomeric state populated via (^{12}C, 3n) at VICKSI in a ^{70}Zn single crystal could only be obtained above 450 K [31]. The combined data, plotted in Fig. 6 on a $T^{1.5}$ scale for simpler interpolation are proof that

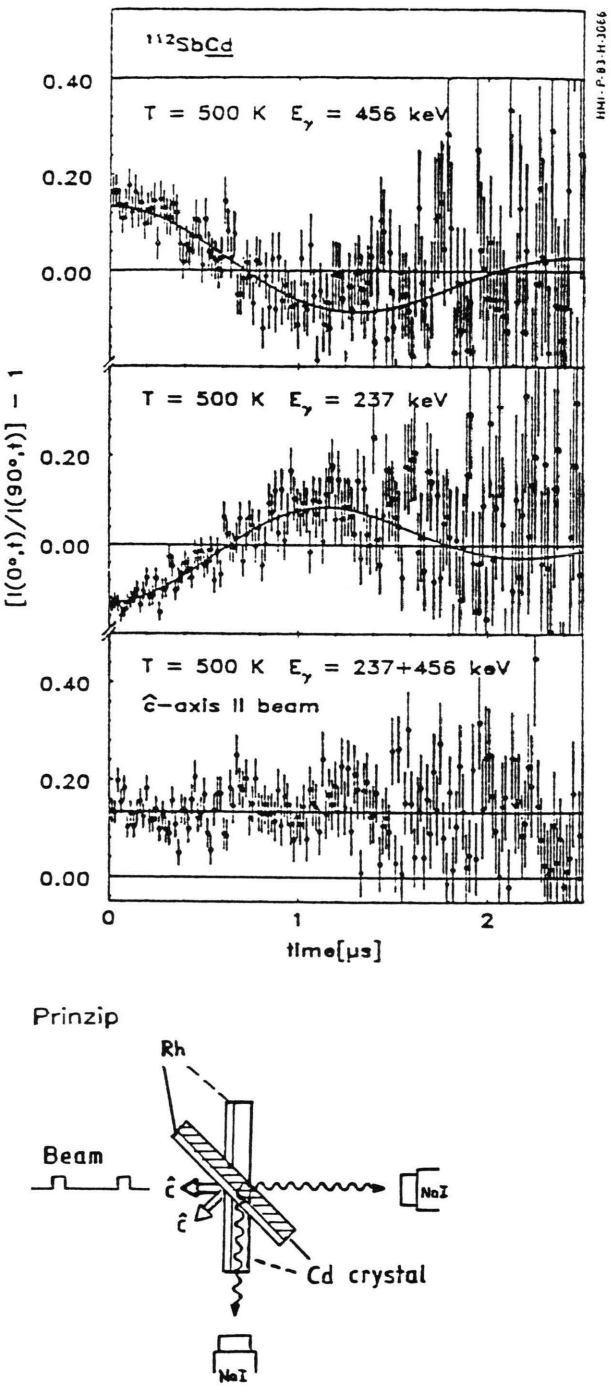

Fig. 5. Quadrupole modulation for ^{112}Sb**Cd** and geometry of experiment.

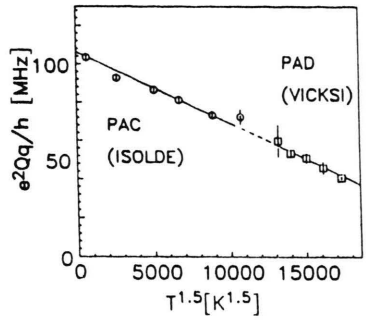

Fig. 6. Results of PAC and PAD experiments for ^{79}Kr**Zn**.

the same (substitutional) lattice site is taken up in both experiments. The expected unusual temperature dependence, more than 3 times stronger than for other impurities in Zn, is clearly demonstrated.

*5. EFG Tensor of Lower Symmetry: ^{80}Rb**Ga***

The crystallographic phase of gallium metal stable at room temperature has an orthorhombic unit cell. The arrangement of atoms can be viewed as a face centered close packing of Ga dimers with their axis tilted 16° from the c-axis in the $a-c$ plane. For a substitutional site the EFG is therefore specified by 3 parameters: q_{zz}, η and an angle β with the z-axis. For Ga matrix atoms these values are known from NQR/NMR experiments [32]. It was interesting to test the application of the PAD technique to the study of impurities in such a more complicated solid.

The 2.4 μs, $I = 6$ isomer of ^{80}Rb was produced in a ^{71}Ga single crystal via (^{12}C, 3n). The modulation pattern in Fig. 7a and its Fourier transform (Fig. 7b) are completely analogous to a NQR spectrum in the time and frequency domain [33]. $e^2 Qq/h = 50.8(1)$ MHz and $\eta = .238(5)$ can be obtained from it with good precision. It is perhaps interesting to mention that in this case the quadrupolar perturbation has been used to determine the spin of the nuclear state involved. An accurate determination of the angle β, however, requires the application of an external magnetic field in a similar way as for NQR. Analysis of the very complex patterns obtained for different field directions gives $\beta = 15(1)°$. The point symmetry at the impurity therefore conforms to the unperturbed lattice, giving strong support to the assumption of a

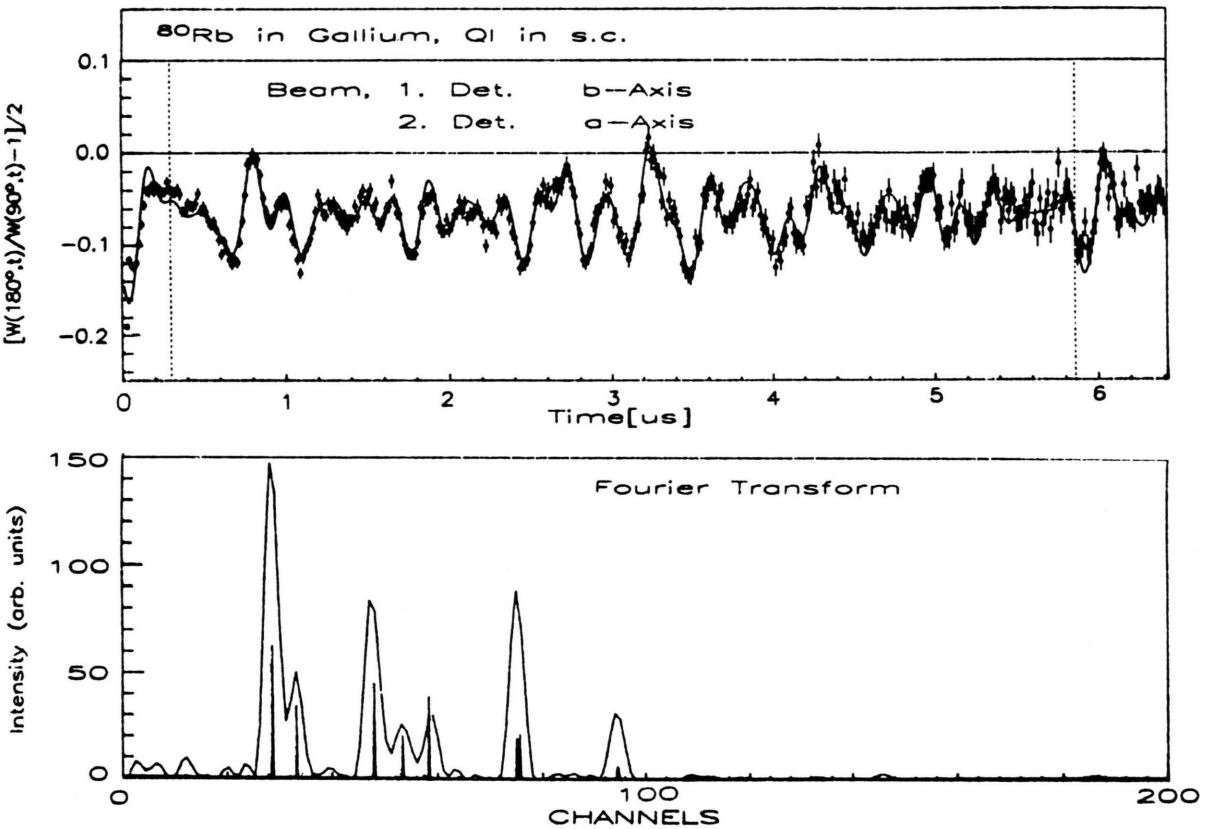

Fig. 7. a) Time spectrum for quadrupole modulation for ^{80}Rb in Ga single crystal. b) Fourier transform of Fig. 7a.

substitutional replacement. The close agreement of the angle β with the lattice value, however, seems to be the exception rather than the rule when compared with results for other impurities (Ge, As, Cd, Sn) [34].

C) EFG Systematics

1. sp-Metals

The EFGs are now known for very many impurities in non-cubic metals, primarily through the application of nuclear methods. Several compilations and reviews have been published [35]. Some systematic trends have been discovered, demonstrating that the EFG is directly related to the charge distribution asymmetry in the near neighbourhood of the probe atom. The most important result, however, is that in general the contribution of the conduction electrons overshadows the effect of the ionic cores. At present no theory of electronic structure of metals appears to be able to calculate the EFG with reasonable accuracy for a wide range of systems. It is therefore wise to focus attention on simple probe-matrix combinations.

The groub IIb metals Zn, Cd, Hg all crystallize in a strongly distorted hexagonal lattice that can be derived from a close-packed structure. To eliminate complications due to localized d or f states only sp impurities shall be considered here. In Table 1 the presently known field gradients for 4sp, 5sp and 6sp impurities in the IIb metals are listed. Signs are given only when experimentally determined. In Zn and Cd positive values are found for group I–IV impurities, while for I a negative EFG was measured. For the group Va cases As**Zn** and Sb**Cd** unusually small absolute values were found. These observations suggest a systematic behaviour: Positive EFG for group I–IV, a practically zero-cross-

Table 1. Field gradients for 4sp, 5sp, 6sp probes in Zn, Cd, Hg at $T = 0$ K, all in 10^{17} V/cm^2.

	4sp-Period			5sp-Period			6sp-Period		
	Zn	**Cd**	**Hg**	**Zn**	**Cd**	**Hg**	**Zn**	**Cd**	**Hg**
Ib				+1.7			+14.7	+11.2	
IIb	+3.5	3.1		+7.4	+7.2	6.1	17.7	13.7	9.6
IIIb	5.9	5.3		+12.3	+10.7				
IVa	6.7	3.7	4.9	+14.2	+11.0	12.6			21.2
Va	1.9				0.4				
VIa									
VIIa	6.1	5.0		−15.9	−16.8				
VIIIa	10.5	5.1			6.2				
Ia	<.5	<.6							

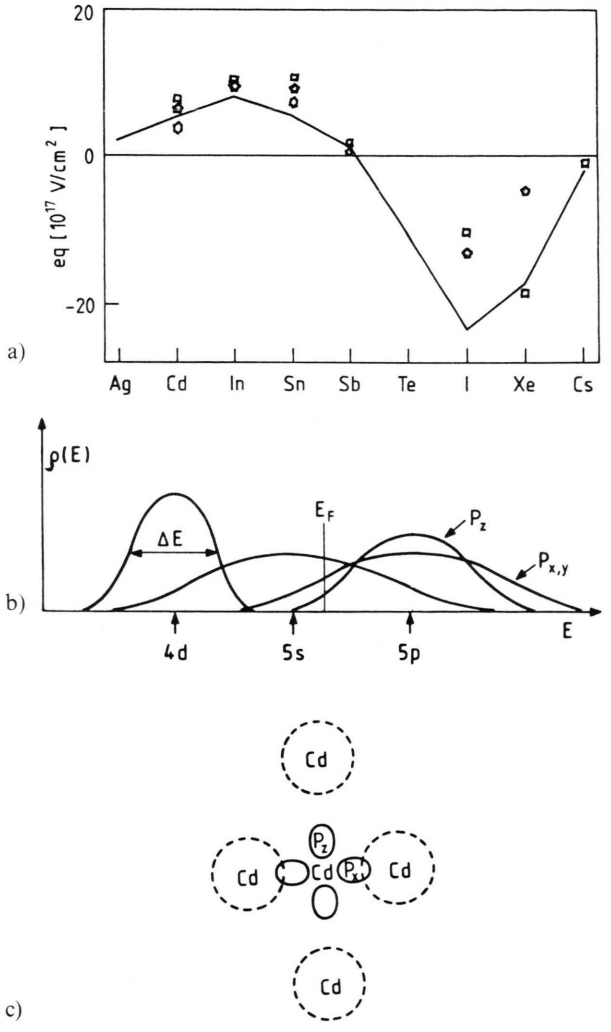

Fig. 8. a) Systematics of EFG in groups IIb metals; (□) 4 sp · 2, (⬠) 5 sp, (⬡) 6 sp/2. The solid line is the model result. b) Local density of states for Cd (model). c) Lattice distortion of Cd (schematic).

ing at group V and negative ones for group VI–VIII probe elements. With this assumption the experimental EFG for 5sp probes in Cd is plotted in Fig. 8a as function of impurity valence. To include the data for 4sp probes (in Zn) on this plot, these have been multiplied by a factor of 2. This is very much suggested by the data of Table 1 and also in line with the relative size of the EFG for a valence p-electron [36]. Similarly a factor of ~ .5 is appropriate for the 6 sp probes (in Hg).

In Fig. 8b a model for the local density of states of a IIb metal (Cd) is shown. It consists of a filled 4d band, a 5s band and 5p bands. The important aspect is that the $5p_z$ band has a smaller width because the overlap to the nearest neighbours is smaller in the z-direction as sketched in Figure 8c. In a simple tight-binding approximation one can obtain the EFG directly as

$$q = \int_0^{E_F} (\tfrac{1}{2}\varrho(p_x) + \tfrac{1}{2}\varrho(p_y) - \varrho(p_z))\,\mathrm{d}E \cdot q_p\,,$$

where q_p is the value for one 5p electron. It may be seen immediately that a positive q results. The electron distribution thus obtained is quite similar to the one assumed in an electrostatic model used to explain the positive Cd (and Zn) field gradient [37].

If then a 5sp impurity is substituted for the central atom in Fig. 8c the atomic 4d, 5s, 5p states will be situated differently with respect to the Fermi level. If the overall nature of the local band structure is not very much changed by this, one can simply shift the local Fermi level on Figure 8b. The resulting q is then zero for E_F at the center of the 5p band, corresponding to a half-filled 5p shell. If one requires neutrality for the impurity atom this would be the case at the group Va element Sb. If the Fermi level moves above the 5p energy, a negative q is obtained. Such a picture can be made somewhat more quantitative by including realistic orbital energies [36] and atomic field gradients for the impurities. The result of such a calculation is included in Fig. 8a showing rather good qualitative agreement with the data. This is evidence that the basic reason for the unusual valence dependence observed is really a local p-orbital phenomenon.

It is interesting to note that the schematic local density of states in Fig. 8b also contains a qualitative explanation for the strong deviation of Cd (and Zn, Hg) from close packing: To first order a Jahn-Teller type distortion of a fictive cubic crystal will

only remove the degeneracy of the p_z and $p_{x,y}$ bands. This enables the system to put more electrons into the band with larger width, thus gaining energy in distorting.

2. Semimetals

With similar reasoning as for the group IIb metals the EFGs for sp impurities in the group Va semimetals As, Sb, Bi are summarized in Figure 9. Here the data are much more sparse and also values for impurities from a group different from the matrix had to be included, applying a correction factor of .5, 1, and 2 for period 4, 5, and 6 probes. A similar trend may be observed as in the IIb matrices, with a zero-crossing at about group IIIa. This trend can be explained in a straightforward way using a covalent bonding picture [38]. The tendency that the normalized EFGs generally decrease going from As through Sb to Bi as matrix is seen as a direct consequence of the decreasing deviation from close packing. A disturbing fact is the observation that in Sb opposite signs for the EFG of Hg and Cd have been measured [39, 40]. If these data stand an experimental test, a systematic behaviour would be very hard to find for these semimetals. The unusual temperature dependence for Cd**Sb** discussed below further complicates the picture. That the zero-crossing for Bi as matrix is shifted more towards group IV may be an indication that Bi is more metallic than the other two semimetals.

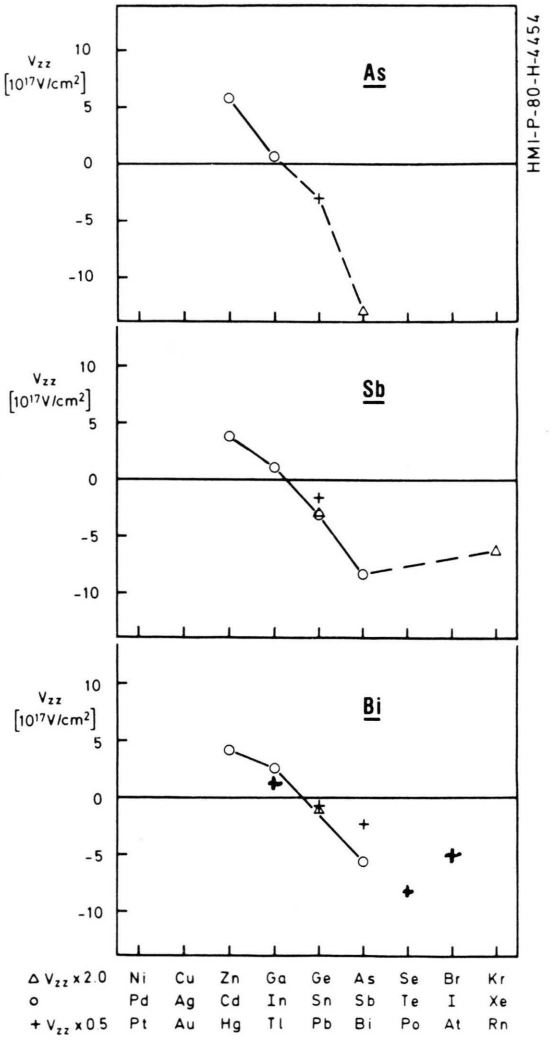

Fig. 9. Systematic of EFG in group Va semimetals. Lines to connect points.

3. d-Elements

A considerable amount of experimental data also exists for d-probes as impurities, mostly in other d-elements. It has been demonstrated clearly that an initially proposed "universal" correlation [41] between ionic and electronic contribution is widely violated for such systems, just as for the sp-elements discussed above. Some modified systematic trends have been postulated [42]. It will be interesting to see if the qualitative understanding reached for the sp-elements can be extended to the d (and f) probes.

4. Anomalies

In all the cases studied up to now the EFG at a substitutional impurity has been found to conform to lattice symmetry. Due to the short range nature of the interactions leading to the field gradients, these have generally been found to be little affected by impurities in metals. Two exceptions to these rules have been found that could be a clue to a significant local electronic structure change at the probe nuclei:

a) For the EFG at Rh in the hexagonal Y lattice a value of $\eta = 0.5$ has been measured [43]. This could imply a strong local symmetry breaking, possibly connected with localized d-states at the Rh atom.

b) The EFG at Cd in Sb is strongly influenced by impurities like Cd or In. Even 0.1% can lead to a change by 50% [44]. This observation, pointing to a

localized electronic state at the Cd probe in the semimetal Sb, is certainly also connected with the unusual temperature dependence [44] of the EFG in this system.

D) Applications

1. Lattice Relaxation in Alloys

Since the EFG is closely connected to the geometrical arrangement of the environment of the probe atom, it is influenced even by small changes of the lattice structure. According to the schematic density of states for Cd in Fig. 8 one would expect that when taking electrons out of the conduction band the force leading to distortion should become smaller because fewer electrons will be in the p-band. Therefore the c/a ratio should decrease on alloying with monovalent impurity atoms (Ag, Au) while it should increase for trivalent impurities. Precisely this effect has actually been observed quite some time ago for Zn alloys.

For Cd alloys the corresponding shifts in $e^2 Qq/h$ on alloying could be quite readily observed [45]. Furthermore, a frequency distribution is induced on alloying in proportion to the frequency shift. This is evidence that the lattice relaxation around an impurity of different valence is rather long-ranged and highly anisotropic.

2. Diffusion in Alkali Alloys

Among the simplest non-cubic metallic systems for the study of EFGs would be alkali-alkali alloys. Here one can reach a quantitative understanding with present day theories. Unfortunately experimenting with these systems has considerable difficulties. Using PAD in a magnetic field it has been possible to measure the quadrupolar frequency distribution for ^{80}Rb in several alloys [46]. For a representative case the frequency distribution width is shown in Fig. 10 as function of temperature. Here the random atomic distribution of the two components leads to non-vanishing EFGs even in the overall cubic alloys. Above 180 K significant changes are observed. They can be related to the onset of atomic diffusion in this temperature range, thus resulting in a motional narrowing. The concentration dependence of the distribution width follows approximately a $\sqrt{c(1-c)}$ relationship.

3. Point Defects: ^{111}InAl

The study of point defects in metals is certainly the area where the nuclear methods have been applied most successfully. Vacancies or interstitials in the neighbourhood of the probe atom will create EFGs even in cubic metals. The defects are produced in various ways. Implantation, p, α, n, e^--irradiation, quenching, cold-work, and nuclear recoil have been used. In most cases the experiment has to be performed such that the defect is a near neighbour of the probe atom. The case to be discussed, vacancy trapping at In in Al, is one of $\sim$ 100 existing examples.

In Fig. 11 a three PAC spectra of $^{111}\text{In} \rightarrow {}^{111}\text{Cd}$ in an Al single crystal are shown [47]. After cyclic torsion at 77 K the weak slope indicates more crystal imperfections created far from the probe. At 210 K the defects can migrate and be trapped at In. The pattern observed is characterized by $\eta = 0$, $e^2 Qq/h = 133$ MHz. Measurements at different angles have shown that the EFG axis is along [111]. Since this same frequency is also observed on quenching of Al [48], the vacancy type nature is proven. The most straightforward structural model would be a trapped divacancy, leading to the configuration shown in Figure 11 b. At higher temperatures the defect is no more observed clearly due to detrapping.

Together with similar experiments using e^--irradiation to produce trapped interstitials one can get detailed information about the nature of the

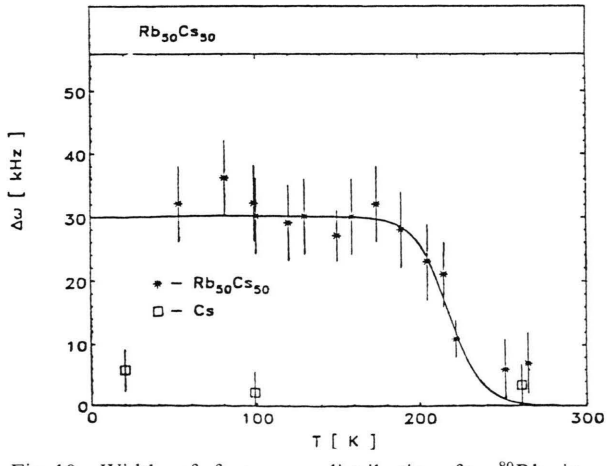

Fig. 10. Width of frequency distribution for ^{80}Rb in $Rb_{50}Cs_{50}$.

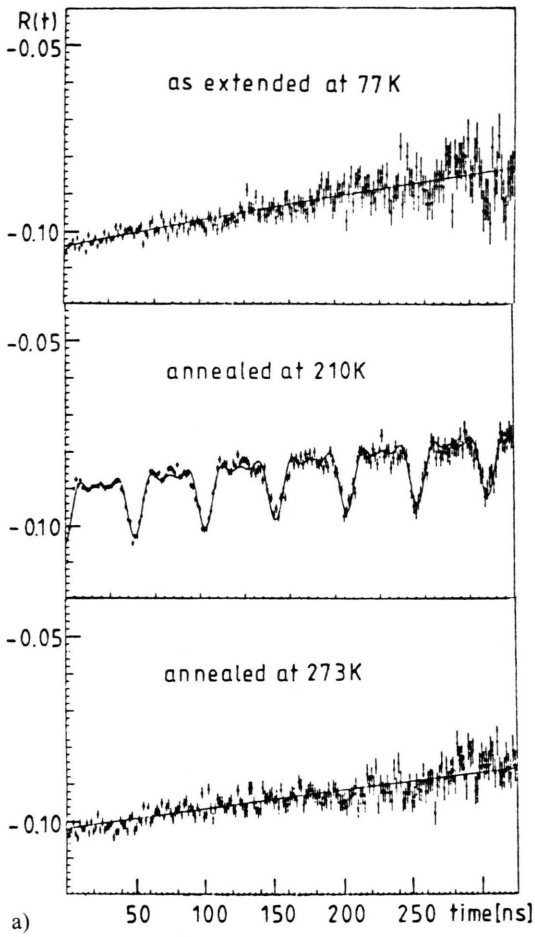

different annealing stages in Al. In general the evidence from the nuclear techniques may be summarized that no support is found for the two types of interstitials postulated for fcc (and hcp) metals.

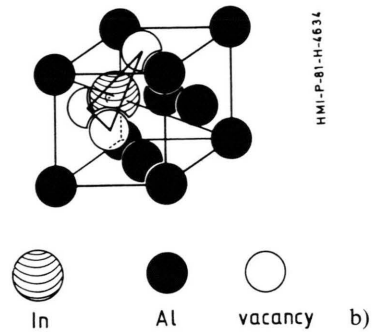

Fig. 11. a) PAC spectra for $^{111}In \rightarrow {}^{111}Cd$ in cold worked Al. b) Proposed structure of trapped divacancy.

4. Surface Studies

Since the nuclear methods require only a relatively small number of atoms, they are ideally suited to study interfaces or surfaces. It should be quite straightforward to investigate isolated atoms at a single crystal surface. Unfortunately the technical problems are rather formidable. Recently a first experiment by PAC of that type has been successful and the EFG for one system, ^{111}Cd on Mo (110), could be measured [49]. More sophisticated experiments to study defects or diffusion on surfaces are clearly possible.

The first PAC experiment at surfaces was the determination of the ^{111}Cd EFG in an In monolayer on In [50]. Furthermore the EFGs for Li and Na on W (110) have been measured recently by a different technique [51]. There seems to be a completely new research field coming up, nuclear surface physics.

[1] F. Bloch, W. W. Hansen, and M. Packard, Phys. Rev. **70,** 474 (1946). – E. M. Purcell, W. C. Torrey, and R. V. Pound, Phys. Rev. **69,** 37 (1946).
[2] R. V. Pound, Phys. Rev. **79,** 685 (1950). – W. G. Dehmelt and H. Krüger, Naturwissenschaften **37,** 111 (1950).
[3] K. Alder, Phys. Rev. **84,** 369 (1951).
[4] R. J. Blin-Stoyle and M. A. Grace, Oriented Nuclei, Encyclopedia of Physics, Vol. XLII (S. Flügge, ed.), Springer, Berlin 1957.
[5] P. B. Treacy, Nucl. Phys. **2,** 239 (1956).
[6] D. Connor, Phys. Rev. Letters **3,** 429 (1959).
[7] R. C. Mössbauer, Z. Physik **151,** 124 (1958).
[8] J. Christiansen, ed., Hyperfine Interactions of Radioactive Nuclei, Springer, Berlin 1983.
[9] See e.g. Proceedings of Inf. Conf. on Hyperfine Interactions (1977 Madison, 1980 Berlin, 1983 Groningen), published in Hyperfine Interactions 4, 9/10, 15/16.
[10] R. M. Steffen and H. Frauenfelder, in: Perturbed Angular Correlations, p. 1 (E. Karlsson, E. Matthias, and K. Siegbahn, eds.), North Holland, Amsterdam 1964. – R. M. Steffen, in: Angular Corrections in Nuclear Disintegration, p. 1 (H. v. Krugten and B. van Nooijen, eds.), University Press, Rotterdam 1971.
[11] R. S. Raghavan, P. Raghavan, and E. N. Kaufmann, Phys. Rev. Letters **31,** 111 (1973).
[12] O. Klepper, E. N. Kaufmann, and D. E. Murnick, Phys. Rev. **C 7,** 1691 (1973).
[13] M. Hass, E. Dafni, H. H. Bertschat, C. Broude, F. D. Davidowski, G. Goldring, and D. M. S. Lesser, Nucl. Phys. A **414,** 316 (1984).

[14] H. L. Ravn, Phys. Reports **54,** 201 (1979).
[15] W. Busse, B. Martin, R. Michaelsen, W. Pelzer, D. Renner, B. Spellmeyer, and K. Ziegler, Nucl. Instrum. Met. **184,** 229 (1981).
[16] M. Menningen, H. Haas, H. H. Bertschat, R. Butt, H. Grawe, R. Keitel, S. Sielemann, and W.-D. Zeitz, Phys. Letters **77 A,** 455 (1980).
[17] J. Bleck, R. Butt, H. Haas, W. Ribbe, and W.-D. Zeitz, Phys. Rev. Letters **19,** 1371 (1972).
[18] R. S. Raghavan and P. Raghavan, Phys. Letters **36 A,** 313 (1971).
[19] J. Christiansen, P. Heubes, W. Keitel, W. Sandner, and W. Witthuhn, Z. Phys. **B 24,** 177 (1976).
[20] T. Butz, B. Lindgren, and H. Saitovich, Hyperfine Interactions **7,** 81 (1979).
[21] R. S. Raghavan, P. Raghavan, and J. H. Friedt, Phys. Rev. Letters **30,** 10 (1973).
[22] O. Echt, H. Haas, E. Ivanov, E. Recknagel, E. Schlodder, and B. Spellmeyer, Hyperfine Interactions **2,** 230 (1976).
[23] P. Herzog, K. Freitag, M. Reuschenbach, and B. Walitzki, Z. Phys. **A 294,** 13 (1980).
[24] H. Bertschat, O. Echt, H. Haas, E. Ivanov, E. Recknagel, E. Schlodder, B. Spellmeyer, M. Ionescu-Bijor, A. Iordachescu, B. Pascovici, D. Plostenaru, and S. Vajda, Hyperfine Interactions **2,** 326 (1976).
[25] O. Echt, H. Haas, E. Ivanov, E. Recknagel, E. Schlodder, and B. Spellmeyer, Hyperfine Interactions **2,** 232 (1976).
[26] H. Haas, M. Menningen, H. Andreasen, S. Damgaard, H. Grann, F. T. Peterson, and G. Weyer, Hyperfine Interactions **15/16,** 215 (1983).
[27] R. E. Shroy, A. K. Gaigales, G. Schatz, and D. B. Fossan, Phys. Rev. **C 19,** 1324 (1979).
[27] W. Semmler, H. Haas, H.-E. Mahnke, and R. Sielemann, Hyperfine Interactions **15/16,** 219 (1983).
[29] H.-E. Mahnke, E. Dafni, M. H. Rafailovich, G. D. Sprouse, and E. Vapirev, Phys. Rev. **126,** 493 (1982).
[30] H. Haas and H. H. Bertschat, Hyperfine Interactions **9,** 273 (1981).
[31] H. G. Devare, H. Haas, H.-E. Mahnke, M. Menningen, W. Semmler, R. Sielemann, and W.-D. Zeitz, Annual Report P 1981, p. 99, Hahn-Meitner-Institut Berlin, HMI-373.
[32] M. I. Valic and D. L. Williams, J. Phys. Chem. Solids **33,** 2337 (1966).
[33] M. Menningen, H. Grawe, H. Haas, W.-D. Zeitz, and R. Keitel, Annual Report P 1979, p. 80, Hahn-Meitner-Institut Berlin, HMI-318.
[34] M. Menningen, Diplomarbeit, Fachbereich Physik, FU Berlin 1977.
[35] E. N. Kaufmann and R. J. Vianden, Rev. Mod. Phys. **51,** 161 (1979). – R. Vianden, Hyperfine Interactions **15/16,** 1081 (1983).
[36] S. Fraga, J. Karwowski, and K. M. S. Saxena, Handbook of Atomic Data, Elsevier, Amsterdam 1976.
[37] E. Bodenstedt and B. Perscheid, Hyperfine Interactions **5,** 991 (1978).
[38] H. Haas and M. Menningen, Hyperfine Interactions **9,** 277 (1981).
[39] J. C. Soares, K. Krien, P. Herzog, H. R. Folle, K. Freitag, F. Reuschenbach, M. Reuchenbach, and R. Trzcinski, Z. Phys. **B 31,** 395 (1978).
[40] E. N. Kaufmann, K. Krien, W. Pielen, and R. Vianden, Hyperfine Interactions **15/16,** 237 (1983).
[41] P. Raghavan, E. N. Kaufmann, R. S. Raghavan, E. J. Ansaldo, and R. A. Naumann, Phys. Rev. **B 13,** 2835 (1976).
[42] H. Ernst, E. Hagn, E. Zech, and G. Eska, Phys. Rev. **B 19,** 4460 (1979).
[43] R. Vianden and P. M. J. Winand, Hyperfine Interactions **9,** 339 (1981).
[44] H. Barfuß, G. Böhnlein, F. Gubitz, W. Kreische, and B. Roseler, Hyperfine Interactions **15/16,** 815 (1983).
[45] M. Menningen, H. Haas, and Ch. Stenzel, Annual Report P 1984, p. 122, Hahn-Meitner-Institut Berlin, HMI-B-Nr. 420.
[46] Ch. Stenzel, H. Haas, and H. H. Bertschat, Annual Report P 1984, p. 120, Hahn-Meitner-Institut Berlin, HMI-B-Nr. 420.
[47] H. G. Müller, Proc. of the Yamada Conf. on Point Defects in Metals, J. Takamura, M. Doyama and M. Kiritani, eds., Univ. Press Tokyo, p. 216 (1982).
[48] H. Rinneberg and H. Haas, Hyperfine Interactions **4,** 678 (1978).
[49] H. Haas, M. Menningen, V. Marx, and Ch. Stenzel, Annual Report P 1984, p. 123, Hahn-Meitner-Insitut Berlin, HMI-B-Nr. 420.
[50] W. Körner, W. Keppner, B. Lehndorff-Junges, and G. Schatz, Phys. Rev. Letters **49,** 1735 (1982).
[51] B. Horn, E. Koch, and D. Fick, Phys. Rev. Letters **53,** 364 (1984).